HTD-Vol. 317-1, 1995 IMECE
Proceedings of the ASME Heat Transfer Division

A STUDY OF DOUBLE-DIFFUSIVE ROLLOVER IN CYLINDRICAL ENCLOSURES

Tetsuo Munakata* and Noam Lior
Department of Mechanical Engineering and Applied Mechanics
University of Pennsylvania
Philadelphia, PA

Ichiro Tanasawa
Institute of Industrial Science
University of Tokyo
Tokyo, Japan

ABSTRACT

The spontaneous destabilization of stably-stratified fluids due to the reversal of the density gradient, caused by heat and/or mass transfer, sometimes in conjunction with evaporation, is known as "rollover". This phenomenon occurs in nature and in industrial processes, best known in the storage of liquefied natural gas (LNG). This study models the process by numerically solving the transient momentum, energy, and mass transfer equations for a binary solution in a cylindrical enclosure. Initially the fluid is stably stratified, with the upper layer having a higher concentration of the lighter component. Heating through the walls is then applied, resulting in buoyancy-driven convection accompanied by heat and mass transfer, and often finally in rollover. Computations are performed for a Prandtl number of 30, Schmidt number of 5500 and for the range of modified thermal Rayleigh numbers of $(1.64)10^9 \le Ra^*_T \le (9.02)10^9$ and solutal Rayleigh numbers of $(4.415)10^9 \le Ra_s \le (1.776)10^{10}$. As expected, the tendency to rollover increases with increasing Ra^*_T and decreases with increasing Ra_s. The most important mechanism which triggers rollover is buoyancy-driven penetration of the lower liquid into the upper layer along the heated side wall. The basic phenomena in the cylindrical and rectangular enclosures were found to be similar, but the interface descent velocity and the intensity of mixing in the cylindrical enclosure are higher, resulting in somewhat different times to onset of rollover.

NOMENCLATURE

C	Dimensionless concentration = $\frac{C' - C'_L}{\Delta C'}$	
C'	Concentration, kg solute/kg solution	
D	Diffusivity of the solute in the solution, m^2/s	
g	Gravitational acceleration, 9.8 m/s^2	
H	Height of the container, m	
k	Thermal conductivity, W/m K s	
Pr	Prandtl number of the solution = ν/α	
$\dot{q}$	Heat flux, W/m^2 s	
r	Dimensionless radial coordinate = r'/H	
r'	Radial coordinate, m	

*On scholarly leave from The Mechanical Engineering Laboratory, AIST, MITI, Tsukuba, Japan

R Radius of the container, m

Ra_s Solutal Rayleigh number = $\frac{g\beta_s H^3 \Delta C'}{\nu D}$

Ra^*_T Modified Thermal Rayleigh number = $\frac{g\beta_T H^4 \dot{q}}{\alpha \nu k}$

R_S Stability parameter = $\beta_s \Delta C / \beta_T \Delta T$

Sc Schmidt number = ν/D

T Dimensionless temperature = $\frac{T' - T'_i}{\dot{q}H/k}$

T' Temperature, K

T'_i Initial temperature, K

t Time, s

V_r, V_z Velocity components in the r and z directions, respectively, m/s

x Dimensionless horizontal coordinate for rectangular enclosure

z Dimensionless axial (or height) coordinate = z'/H

z' Axial coordinate, m

α Thermal diffusivity, m^2/s

β_S Volumetric expansion coefficient for concentration, $(kg)^{-1}$

β_T Volumetric expansion coefficient for temperature, $(K)^{-1}$

ΔC Driving concentration difference, kg/kg

$\Delta C'$ Initial concentration difference between the upper and lower fluid layers = $C'_H - C'_L$, kg/kg

ΔT Driving temperature difference, K

$\Delta T'$ $= T'_{i,H} - T'_{i,L}$

ν Kinematic viscosity, m^2/s

ρ Density, kg/m^3

τ Dimensionless time = $\frac{t}{H^2/\nu}$

ω Vorticity

ψ Stream function

Subscripts

H for the upper fluid layer, $H/2 \le z \le H$

L for the lower fluid layer, $0 \le z \le H/2$

Superscripts

Area-averaged over r or x

Volume-averaged

1. INTRODUCTION

The spontaneous destabilization of stably-stratified fluids due to the reversal of the density gradient, caused by heat and/or mass transfer, sometimes in conjunction with evaporation, is known as "rollover". In this process the heat and/or mass transfer cause the densities of the bottom and top fluid layers to approach equality or may even cause the reversal of the density gradient, with the top layers becoming heavier than the bottom ones. This equalization of densities or reversal of gradients causes, sometimes suddenly, strong mixing of the layers, at times to the extent of literal "rolling" of the bottom layers above the top ones. This has been observed in many engineering and natural circumstances, such as in liquefied natural gas (LNG) storage tanks, heat storage tanks, solar ponds, and ocean and atmospheric circulation. It can also occur in material processing such as in the melt of semiconductor materials and metallic alloys, and in liquid hydrocarbon mixture fires.

One good and technologically important example is rollover in LNG storage tanks and is described here in more detail (cf., Sarsten, 1972; Acton and Van Meerbeke, 1986) focusing on the processes which lead to destabilization. Heat flows from the ambient into the colder liquid through the tank walls. The partial pressures of the species in the vapor space above the liquid ("ullage") are often lower than those in the liquid. This is because of the gradual rise in the temperature of the liquid, the relatively slow rate of diffusion of some of the species through the liquid towards the free surface, and some evacuation of the species from the vapor space due to gas use and venting. The heat flow rises the liquid temperature. This, together with the lower partial pressure in the vapor space leads to evaporation at the free surface, or even to bubble nucleation and evaporation at some depth. The temperature rise of the lower layers decreases their density, giving

rise to natural convection (in the form of rolls) even if the fluid is initially stably stratified and the heat flow is only through the tank walls which are parallel to the gravity vector (cf. Lior and Fujii, 1991). Evaporation has heat and mass transfer consequences which affect the density of the upper layer: the temperature drop increases its density, while the removal of the evaporating species may either increase or decrease the layer density, depending on the molecular weight of the evaporated species. For example, if nitrogen is present in the LNG, it would boil off preferentially, and since it has a higher molecular weight than methane (usually a dominant hydrocarbon in LNG) the density of the upper layer would decrease. The opposite happens in the absence of significant amounts of nitrogen: the lighter hydrocarbon components, such as methane, would be evaporated preferentially, thus increasing the density of the upper layer. Another common impetus for destabilization is when a fresh layer of higher-density LNG is added to an existing one (i. e., to the so-called "heel"). In summary, transient double-diffusive phenomena, evaporation, buoyancy, heat exchange with the environment, and fluid mechanics of mixing when fresh LNG is added to the heel, determine stability and mixing, and thus rollover in LNG storage tanks.

Rollover and the associated vigorous mixing result in a rapid increase in the rate of evaporation in LNG storage tanks, especially if the lower layer was superheated relative to the pressure in the tank vapor space. This is accompanied by a rapid rise of the gas pressure in the tank, causing a significant safety problem.

One of the earliest and best-known examples is an incident at La Spezia in Italy in 1971. Eighteen hours after adding a new LNG into the tank, the pressure in the tank rose abruptly by 40%, safety valves remained raised for 1.5-2 hours and 185,000 kg boil-off gas was released into the atmosphere. It has been reported that the differences in densities and temperatures between the two (initially stored and newly added) LNGs were 9 kg/m^3 and 2 K, respectively. Many incidents of different magnitude of severity have been reported since.

The definition and evaluation of a stability criterion for such density-stratified layers is obviously of central importance in the study of rollover. For two such double-diffusive layers, some researchers (e.g., Turner, 1965,1973; Takao and Narusawa, 1980; Newell and Von Driska, 1983; Sugawara et. al. 1984; Muro et. al., 1986) used a "stability parameter" R_s, defined as $R_s=\beta_s\Delta C/\beta_T\Delta T$, where β_s and β_T are the coefficient of volumetric expansion due to concentration and temperature, respectively, and ΔC and ΔT are the difference in concentrations and temperatures between the two liquid layers, respectively.

Use of the stability parameter is qualitatively reasonable because it represents a ratio between two forces which affect stability, $\beta_s\Delta C$ which is due to the concentration effect on density, and $\beta_T\Delta T$ due to the temperature effect. This parameter, however, does not seem so effective in interpreting the phenomena occurring at the boundary between the two liquid layers. Morioka and Enya (1981, 1984) have observed that the flow boundary layer along the lower vertical wall penetrates into the top layer when the density difference between the two liquids reaches nearly zero, and then the interface between the two liquids descends slowly. Opposite results were found in the 2-dimensional (rectangular enclosure) numerical analysis by Shi (1990) who assumed the layers to be liquid nitrogen and oxygen, and found that rollover occurred due to upper-core flow penetration into the interface.

In a previous paper, two of the authors (Munakata and Tanasawa, 1994) have reported the results of a numerical study of such a rollover phenomenon in a rectangular enclosure, and have at least qualitatively verified it by experimental findings of their research group (Arita et al., 1992). This paper expands the investigation to the cylindrical enclosure, a configuration which is not only more realistic for storage tanks but also results in rather different flow, temperature and concentration fields, and thus in different rollover onset conditions.

2. THE MODEL

The model used for the numerical simulation covered in Sections 2-5 is illustrated in Fig. 1. Initially, the vessel, of a radius R equal to its half-depth (H/2), contains two binary-solution fluid layers of the same solvent and solute, temperature, and depth (H/2), which are density-stratified because of having different concentrations of the solute. The top surface is free, the top and bottom surfaces of the fluid are adiabatic, no evaporation exists, the Marangoni effect at the free surface is neglected, and the fluid layers are heated from the side wall. It is assumed that the flow, temperature and concentration fields are axisymmetric with respect to the z-axis.

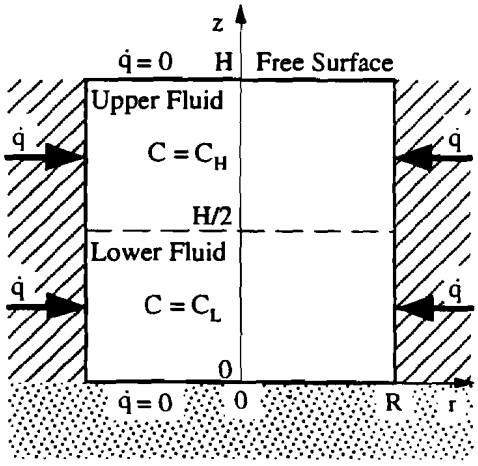

Fig.1 The model for rollover analysis.

The Soret and Dufort effects are assumed to be much weaker than heat conduction and molecular diffusion, and are thus neglected.

The describing equations (in vectorial form) and the initial and boundary conditions are shown below, and the nondimensional parameters used are listed in the Nomenclature (more detail about their derivation can be found in Munakata and Tanasawa, 1994).

(1) The describing equations

The momentum equation using vorticity

$$\frac{\partial\omega}{\partial\tau} + V_r\frac{\partial\omega}{\partial r} + V_z\frac{\partial\omega}{\partial z} - \frac{2V_r}{r}\omega = \left(\frac{\partial^2\omega}{\partial r^2} + \frac{\partial^2\omega}{\partial z^2} - \frac{1}{r}\frac{\partial\omega}{\partial r}\right) - \frac{Ra_T^*}{Pr}r\frac{\partial T}{\partial r} - \frac{Ra_s}{Sc}r\frac{\partial C}{\partial r} \quad (1)$$

The energy equation

$$\frac{\partial T}{\partial\tau} + V_r\frac{\partial T}{\partial r} + V_z\frac{\partial T}{\partial z} = \frac{1}{Pr}\left(\frac{\partial^2 T}{\partial r^2} + \frac{\partial^2 T}{\partial z^2} + \frac{1}{r}\frac{\partial T}{\partial r}\right) \quad (2)$$

The diffusion equation

$$\frac{\partial C}{\partial\tau} + V_r\frac{\partial C}{\partial r} + V_z\frac{\partial C}{\partial z} = \frac{1}{Sc}\left(\frac{\partial^2 C}{\partial r^2} + \frac{\partial^2 C}{\partial z^2} + \frac{1}{r}\frac{\partial C}{\partial r}\right) \quad (3)$$

The stream function (Poisson) equation

$$\frac{\partial^2\psi}{\partial r^2} + \frac{\partial^2\psi}{\partial z^2} - \frac{1}{r}\frac{\partial\psi}{\partial r} = \omega. \quad (4)$$

The stream-function velocity relation

$$V_r = \frac{1}{r}\frac{\partial\psi}{\partial z}, \quad V_z = -\frac{1}{r}\frac{\partial\psi}{\partial r}, \quad (5)$$

where all the terms are defined in the Nomenclature section.

(2) The boundary conditions

At the bottom (z=0)

$$\psi(\tau,r,0) = \frac{\partial\psi(\tau,r,0)}{\partial z} = \frac{\partial T(\tau,r,0)}{\partial z} = \frac{\partial C(\tau,r,0)}{\partial z} = 0, \quad (6)$$

for $\tau \geq 0$, $0 \leq r \leq R$,

at the center (r=0)

$$\psi(\tau,0,z) = \omega(\tau,0,z) = \frac{\partial T(\tau,0,z)}{\partial r} = \frac{\partial C(\tau,0,z)}{\partial r} = 0, \quad (7)$$

for $\tau \geq 0$, $0 \leq z \leq H$,

at the top (z=H)

$$\psi(\tau,r,H) = \omega(\tau,r,H) = \frac{\partial T(\tau,r,H)}{\partial z} = \frac{\partial C(\tau,r,H)}{\partial z} = 0, \quad (8)$$

for $\tau \geq 0$, $0 \leq r \leq R$,

and at the wall (r=R)

$$\psi(\tau,R,z) = \frac{\partial\psi(\tau,R,z)}{\partial r} = \frac{\partial C(\tau,R,z)}{\partial r} = 0, \quad \frac{\partial T(\tau,R,z)}{\partial r} = 1, \tag{9}$$

for $\tau \geq 0$, $0 \leq z \leq H$.

(3) The Initial Conditions ($\tau = 0$)

$$\psi(0,r,z) = \omega(0,r,z) = T(0,r,z) = 0 \text{ for } 0 \leq r \leq R, \ 0 \leq z \leq H, \tag{10}$$

and, to avoid numerical problems associated with the initial concentration step function, the initial concentration distribution is taken to be the analytical solution of the transient one-dimensional diffusion equation with the identical initial step-function concentration

$$\begin{aligned} C(0,r,z) &= 0 \quad \text{for } 0 \leq r \leq R, \ 0 \leq z \leq H/2, \text{ and} \\ C(0,r,z) &= 1 \quad \text{for } 0 \leq r \leq R, \ H/2 \leq z \leq H, \end{aligned} \tag{11}$$

which is

$$C(\tau,z) = \frac{1}{2} erfc\left(\frac{\frac{1}{2} - z}{2\sqrt{\frac{\tau}{Sc}}}\right), \tag{12}$$

evaluated at $\tau = 0.1$.

3. THE NUMERICAL PROCEDURES

The previously described governing equations were solved by using the finite difference method. To achieve higher accuracy, we have used a coordinate transformation which places a denser grid next to all interfaces (Fig. 2), third order upwind differences (the K-K method) for the convective terms, and, as described above, the initial concentration distribution based on the exact solution of the one-dimensional pure diffusion problem to avoid the numerical difficulties associated with assuming a step function in the concentration. Excepting the convective term, the other parts of the describing equations were spatially discretized by second order central differences. The ADI method was used for the time integration, and the SOR method was used to solve the Poisson equation. More details about the numerical technique can be found in (Munakata and Tanasawa, 1994).

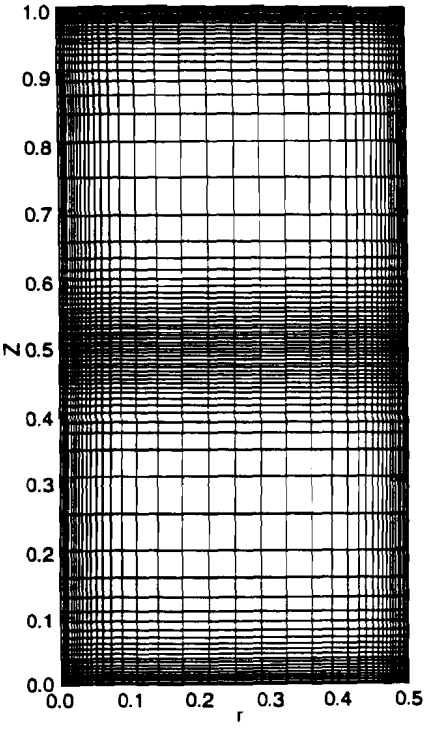

Fig.2 The grid system for the numerical analysis.

The accuracy of the numerical method was determined by examining the effect of mesh size on the obtained results. Figure 3 shows the time-wise variation of stream function (ψ), temperature (T) and concentration C at r=0.4628507, z=0.2514167, for three mesh sizes. The 20×40 mesh obviously gives results which differ significantly from those obtained with finer mesh sizes, and the difference between the 40×80 and 60×120 mesh size results is within 10%. The 40×80 mesh (Fig. 2) was thus used for obtaining the results shown below, computed on a Cray RS6400 multi-processor system.

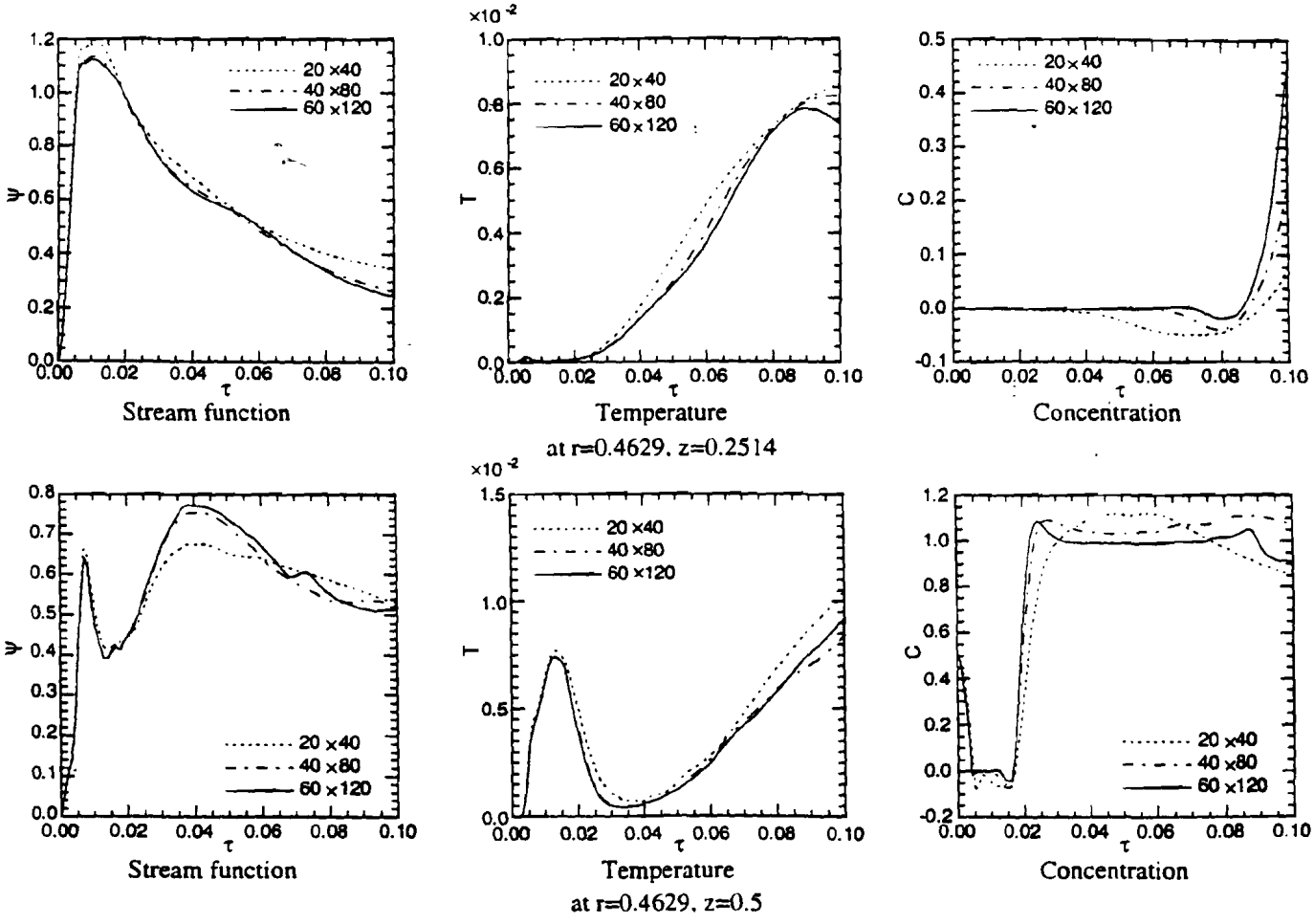

Fig.3 Timewise variation of ψ, T and C for various mesh sizes; Ra_S=4.415×10⁹, Ra^*_T=2.46×10⁹.

4. RESULTS AND DISCUSSION

To compare the results with the previously reported rectangular case (Munakata et al., 1994) which have been validated by our past experimental data (Arita et al., 1992), almost all of the parameters are selected to have the same values. Specifically, the computations were performed assuming that the fluid is a 50% by weight water-ethanol solution in a cylinder with H = 0.08 m. The solution properties, evaluated at room temperature, are listed below.

$\nu = (2.75)10^{-6}$ m²/s $\alpha = (9.5)10^{-8}$ m²/s $D = (5.0)10^{-10}$ m²/s

k = 0.318 W/m K $\beta_T = (8.54)10^{-4}$ K⁻¹ $\beta_s = (2.42)10^{-3}$ wt%⁻¹

ρ_{water} = 1000 kg/m³ $\rho_{ethanol}$ = 800 kg/m³

Based on the above, the Prandtl number is 30 and the Schmidt number 5500. Computations were made for the range $(1.64)10^9 \le Ra^*_T \le (9.02)10^9$ and $(4.415)10^9 \le Ra_S \le (1.766)10^{10}$. The different values of Ra^*_T were obtained by varying the side-wall heat flux $\dot{q}$, and those of Ra_S by varying the initial concentration difference ΔC between the top and bottom fluid layers. We note that Ra^*_T is the modified Rayleigh number, based on heat flux, and

its highest values in this study amount to a temperature-difference-based Rayleigh number of only about $(5.4)10^8$, still in the laminar natural convection regime.

The time-wise variation of the flow, temperature and concentration fields at $Ra_s = (4.415)10^9$ and $Ra^*_T = (1.64)10^9$ shown in Fig. 4 is typical of the obtained results. Initially there are two process-driving forces: (1) The temperature gradient in the fluid near the side wall due to the heat input, which causes a conductive inward heat flux, and (2) the concentration difference (here of ethanol) between the upper and lower layers, which causes downward diffusion. A buoyancy force due to heating through the side walls, moderated by the stabilizing effect of the concentration gradient, generates the two convective cells seen in the Figure, both moving upwards near the side wall and descending close to the center.

Figure 4 shows that at the early times the diffusion of heat and mass is small relative to the natural convection effect. Despite the seemingly distinct upper and lower cells, it can be seen that noticeable fluid transfer occurs between the cells. This commences very soon, moving the lower concentration fluid upwards near the wall with a consequent sharp concentration decrease in the wall boundary layer of the upper region, and by a small concentration increase of the lower region, distributed over a wide part of its interior. Examination of the temperature field shows the effect of convection in transferring heat from the wall into the rolls. This is particularly strong in the upper cell, where it is seen that heat is moved rapidly to the top surface of the enclosure and then downwards in the center region.

Significantly, examination of the transient change of the concentration field demonstrates well the rollover phenomenon, in which the lower liquid layer ascends along the heated wall to penetrate the upper layer, while the upper layer descends in the region further from the wall. In the process the layers mix with each other and "exchange places". This is unlike the findings by Shi (1990) who suggested that rollover resulted from upper core flow into the interface. The difference may be due to the fact that his Pr (2.32) and Sc (0.0754) numbers are much smaller than the ones assumed in our study and in the study by Munakata and Tanasawa (1994). The strong mixing, especially near the top surface but also at the interface between the fluids is also evident.

Qualitatively, these results are similar to the ones obtained for the rectangular enclosure (Munakata and Tanasawa, 1994). The cylindrical flow geometry, however, in which the flow cross section diminishes radially from the wall in, generates a different velocity field and thus different rollover conditions. The wall-heat-transfer induced upward flow, in the largest flow cross sectional area of the cylinder, results in stronger downflow in the inner regions when compared with the rectangular enclosure, as seen in Fig. 5. Both thermal and species mixing at the interfacial and lower regions are also faster. We note that while the equi-potential streamline gradients in the central region of the cylinder (Fig. 4) are smaller than those computed by Munakata and Tanasawa (1994) for the rectangular enclosure, the vertical velocities are actually higher as seen in Fig. 5. This is due to the 1/r multiplier in the velocity-stream-function relationship, eq. (5), which takes a large value in the central region of the cylinder.

The radially-averaged concentration distribution at depth z,

$$\overline{C}(\tau,z) = 4\int_0^{1/2} C(\tau,r,z)\,r\,dr, \qquad (13)$$

is shown at different times for $Ra^*_T=(4.10)10^9$ and $(9.02)10^9$ in Figs. 6 and 7, respectively. Fig. 6 shows clearly that the interface between the two fluid layers becomes more stable when the solutal Rayleigh number increases (i.e., when the initial solutal driving force becomes larger). This is as it should be, since in this case, where initially the higher ethanol concentration and thus lighter fluid is at the top, higher Ra_s indicates a more stable stratification. Analogically, comparison of Fig. 7 with Fig. 6 shows that interface becomes less stable when the thermal Rayleigh number is

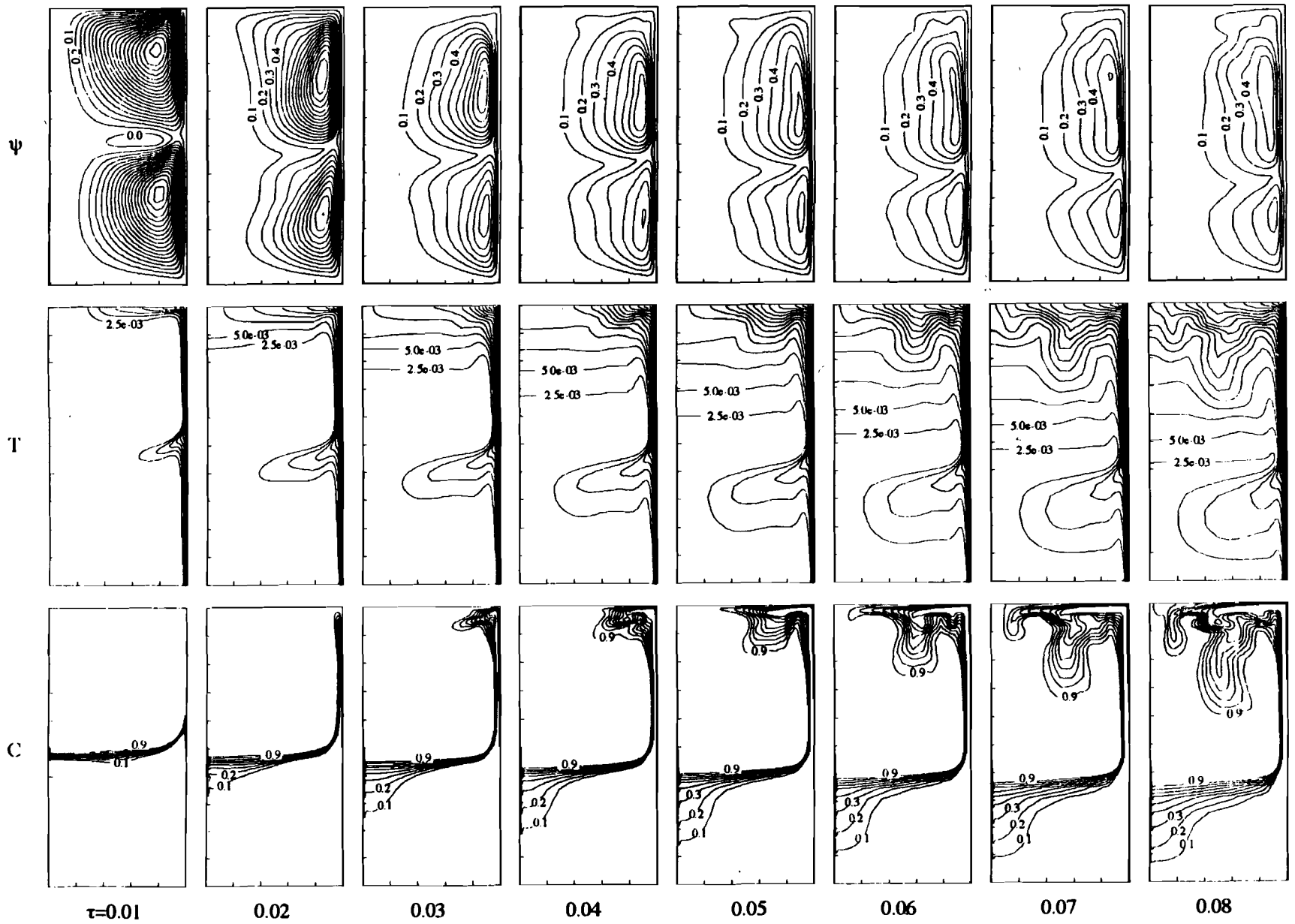

Fig.4 Transient distributions of the stream function (ψ), temperature (T) and conentration (C) for Ra_S=4.415×10⁹, Ra^*_T=1.64×10⁹. The equi-potential lines are separated by Δψ=0.1, ΔT=0.0025, ΔC=0.1.

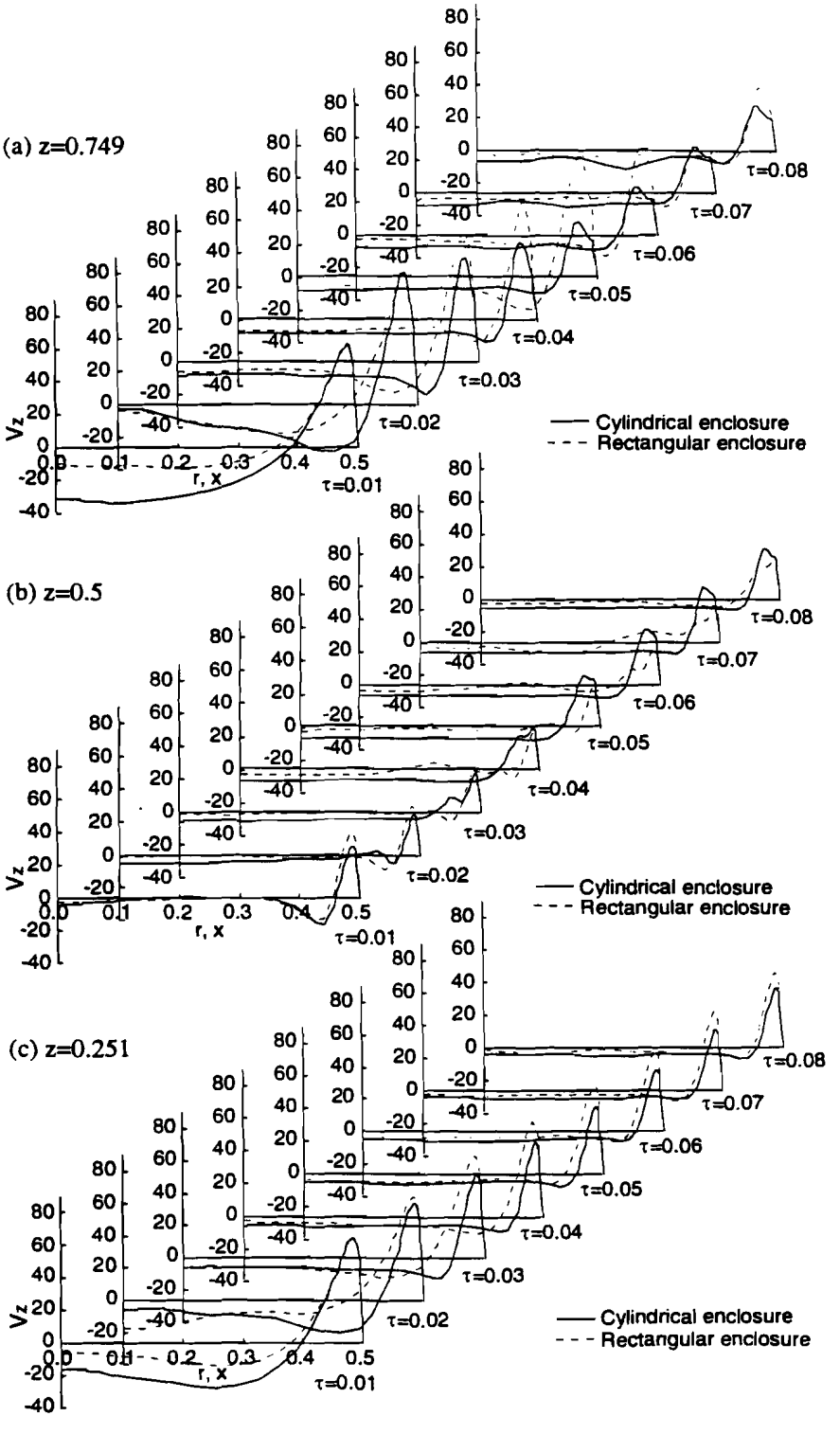

Fig.5 Comparison between the transient vertical velocity distributions in the cylindrical and rectangular enclosures for $Ra_S=4.415\times10^9$, $Ra^*_T=1.64\times10^9$.

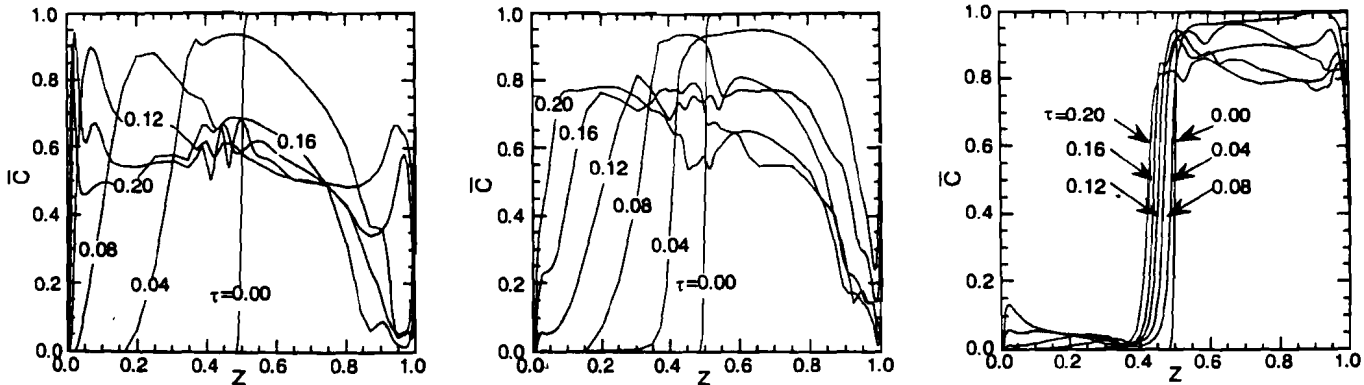

(a) Ra_S=4.415×10⁹ (b) Ra_S=8.83×10⁹ (c) Ra_S=1.766×10¹⁰

Fig.6 The radially-averaged transient concentration distribution with respect to height z, for Ra^*_T=4.10×10⁹.

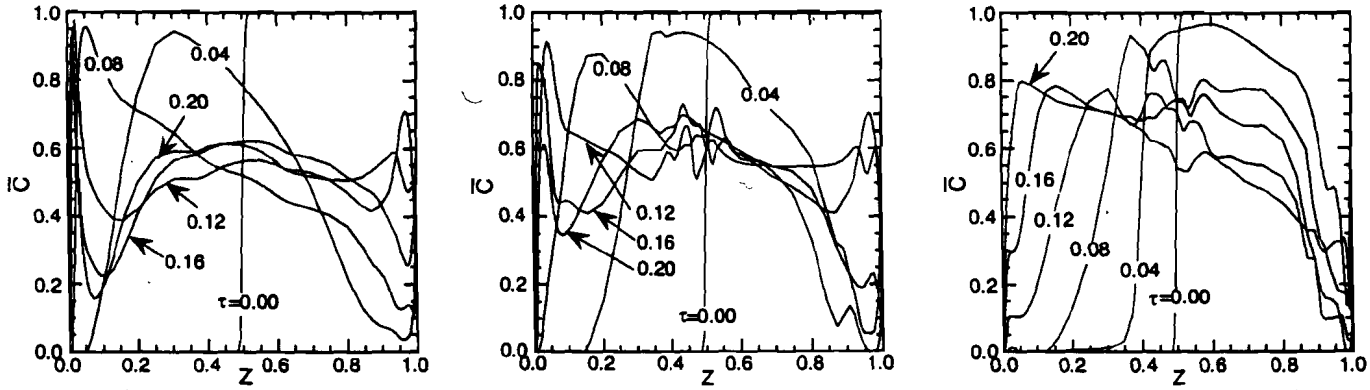

(a) Ra_S=4.415×10⁹ (b) Ra_S=8.83×10⁹ (c) Ra_S=1.766×10¹⁰

Fig.7 The radially-averaged transient concentration distribution with respect to height z, for Ra^*_T=9.02×10⁹.

increased; indeed the increase of the wall heat flux invigorates natural convection. Once again, comparison with the results for the rectangular enclosure show that in cylindrical enclosures the destabilization occurs earlier and the mixing is more vigorous.

To investigate the temporal progression of mixing and rollover, we show in Fig. 8 the transient concentration of the lower and upper fluid regions, volume-averaged over these regions as

$$[\hat{C}(\tau)]_{lower} = 2\int_0^{1/2} \bar{C}(\tau,z)dz, \qquad (14)$$

$$[\hat{C}(\tau)]_{upper} = 2\int_{\frac{1}{2}}^{1} \bar{C}(\tau,z)dz, \qquad (15)$$

where $\bar{C}(\tau,z)$ is obtained from eq. (13).

Examination of Fig. 8 shows that, as expected, the concentration in the upper layer decreases from unity and the concentration in the lower layer increases from zero. For the highest solutal Rayleigh number examined, i.e. the least unstable case computed, the change in the average concentrations is indeed slowest. This is because the convective motion and mixing are weakest. Consistent with that, the rate of change of the average concentrations increases with the thermal Rayleigh number and decreases with the solutal Rayleigh number. For combinations of sufficiently low Ra, and

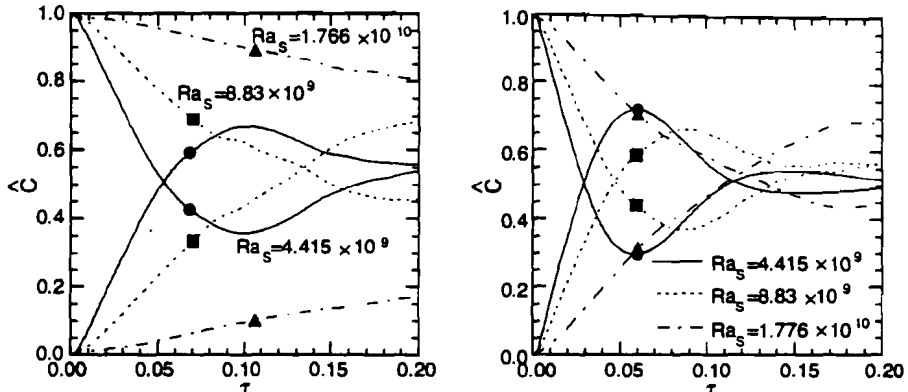

Fig.8 The transient volume-averaged concentration of the lower ($0 \le z \le H/2$) and upper ($H/2 \le z \le H$) fluid regions (note: for each of the values of Ra_S two curves of the same line type are shown, the one starting at the top is for the upper region and the one starting at the bottom is for the lower region).

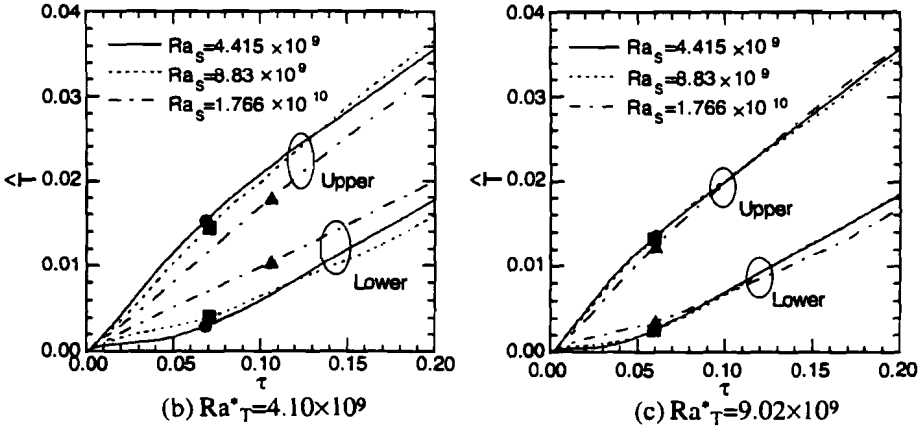

Fig.9 The transient volume-averaged temperature of the lower ($0 \le z \le H/2$) and upper ($H/2 \le z \le H$) fluid regions.

sufficiently high Ra^*_T, the lower and upper region concentrations become equal (at the crossover point of the transient concentration curves in Fig. 8), the lower region concentration then exceeds for a while that of the upper region, the lower region concentration reaches a maximum and the upper region concentration reaches a minimum, and the concentrations of both regions then gradually converge towards each other, ending at the final, fully mixed uniform concentration of the entire enclosure, $\hat{C}=0.5$.

Figure 8 also shows that the layer concentration crossover as well as final homogenization occur sooner when Ra^*_T is larger and Ra_s is smaller, consistent with their effect on the buoyancy-driven convective flow. This can also be seen from the more detailed exposition of the phenomena in the respective curves of Fig. 7.

Figure 9 shows the volume-averaged transient temperature (defined as in eqs. 13-15, with T replacing C) change for the upper and the lower fluid regions. To understand the temperature rise history shown in this Figure, we note that heat is conducted through the wall into both lower and upper regions of the fluid, and that the ensuing natural convection would carry heat upwards. Consequently, when the convection is minimal (the solutal

Rayleigh number is the highest for a given thermal Rayleigh number), the lower fluid layer loses the least heat via convection to the upper layer and thus its temperature rises fastest. This of course coincides then with the proportionately slowest temperature rise of the upper layer seen in Fig. 9. The rate of temperature rise of the lower region thus decreases, and for the upper region it increases, as Ra_s decreases and as Ra^*_T increases. It can also be seen that the lower layer temperature does not rise appreciably at the start for combinations of larger Ra^*_T and lower Ra_s, because of the relatively strong convection which immediately causes flow penetration through the interface from the lower to the upper layer, with consequent heat loss from the lower layer.

Next we consider the prediction of the time to rollover, a parameter of intrinsic interest, but also of particular safety importance in the LNG application. We define the rollover onset time as the time when the interface between the lower and upper layers reaches the top free surface, that is when a point of the top surface (initially at C=1.0) first reaches the concentration C=0.5. The results of the analysis are shown as the solid symbols in Figs. 8 and 9, and are summarized in Fig. 10. Consistent with discussions above, the rollover onset time is seen to diminish as Ra^*_T increases and as Ra_s decreases, and the effect of the magnitude of Ra_s becomes very small for the larger values of Ra^*_T. Comparing (Fig. 11) with our previous results for the rectangular enclosures, it can be seen that the rollover onset times are different: they become shorter (up to -11% here) for the cylindrical vessel as Ra_s increases, they increase with Ra^*_T, and are always longer (by up to 6%) at the higher values of Ra^*_T examined here.

We close this section by noting that this entire study is of introductory and fundamental nature but not yet fully applicable to rollover in LNG tanks. Phenomena not considered in this model, especially evaporation and the Marangoni effect at the free surface, the effects of all species present in the LNG, and the nature of the transient weather-based heat influx, are also likely to have important effects on the rollover onset time. The actual LNG tank sizes would also bring about Rayleigh numbers which may be significantly larger than those considered in this study.

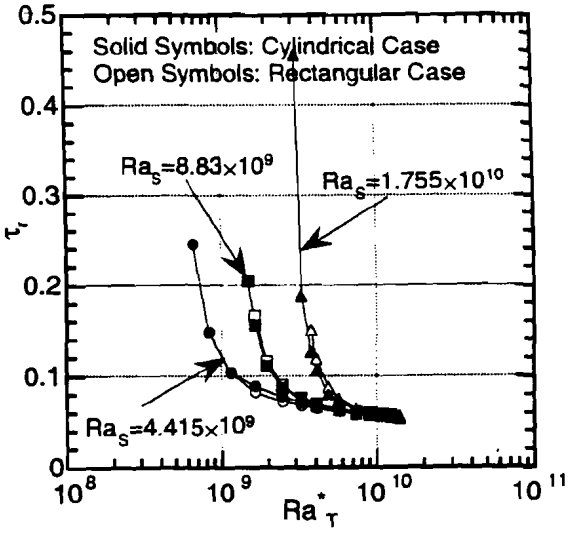

Fig.10 Rollover onset time τ_r.

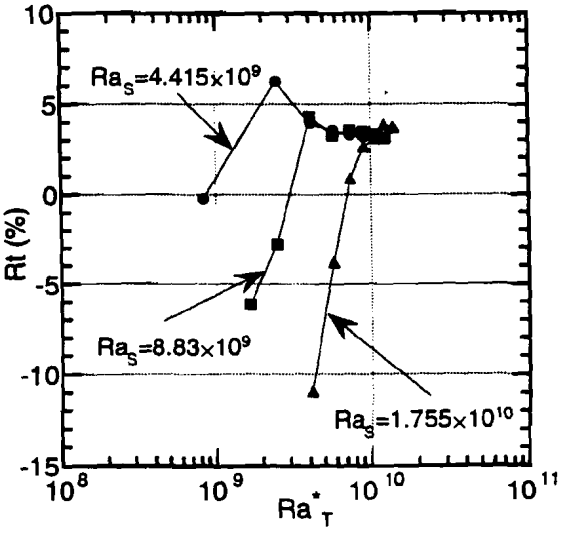

Fig.11 The relative difference Rt between the rollover onset time τ_r for the crlindrical and rectangular enclosures. $Rt \equiv [\{\tau_r(\text{cylindrical}) - \tau_r(\text{rectangular})\}/\tau_r(\text{rectangular})] \times 100$, %

6. CONCLUSIONS

The effect of the initial concentration difference between stably stratified fluid layers, and of the side-wall heat flux, on the rollover phenomena in a cylindrical enclosure have been investigated numerically. The most significant results are:

(1) Heat transfer through the side-walls tends to destabilize a fluid which is initially stably stratified due to concentration differences between its lower and upper regions.

(2) The extent of destabilization and the intensity of the ensuing convective flow and mixing are proportional to the thermal Raleigh number, and inversely proportional to the solutal Rayleigh number (which has a stabilizing effect in this case).

(3) The most important mechanism which triggers rollover is buoyancy-driven penetration of the lower liquid into the upper layer along the heated side wall.

(4) The time to rollover onset becomes shorter as Ra^*_T increases and as Ra_s decreases, and the effect of the magnitude of Ra_s becomes very small for the larger values of Ra^*_T.

(5) The basic phenomena in the cylindrical and rectangular enclosures are similar, but the interface descent velocity and the intensity of mixing in the cylindrical case are higher. The rollover onset time is a few percent shorter for the lower values of Ra_s and higher values of Ra^*_T, and vice versa.

7. REFERENCES

Acton, A. and Van Meerbeke, R.C. 1986, "Rollover in LNG Storage - An Industry View", *8th Int. Conf. on LNG*, Session III, Paper 12, pp.1-21.

Arita, T., Katayama, Y., Hayashi, K., Nishio, S., and Tanasawa, I., 1992, "Fundamental Study on Rollover of Two Density-Stratified Layers of Liquids," *Natural Convection in Enclosures - 1992*, HTD-Vol.198, ASME, pp.67-72.

Lior, N. and Fujii, Y., 1992, "On Conjugate Heat Transfer in Crystal Growth", chapter in *Heat and Mass Transfer in Materials Processing*, I. Tanasawa and N. Lior, ed., Hemisphere Publishing Corp., N. Y., pp. 217-243.

Morioka, M. and Enya, S., 1981, "Natural Convection of Density-Stratified Layers in a Vessel: 1: Observation of Flow Patterns," *Refrigeration* (in Japanese), Vol. 56, No. 644, pp. 529-537.

Morioka, M. and Enya, S., 1984, "Natural Convection of Density-Stratified Layers in a Vessel," *Heat Transfer Japanese Research*, Vol. 12, pp. 48-69.

Munakata, T. and Tanasawa, I. 1994, "Numerical Study on Effect of Initial Concentration Difference on Onset of Rollover," *Proc. 10th International Heat Transfer Conf.*, Vol. 7, pp. 333-338.

Muro, M., Yoshida, M., Iwata, A., Yasuda, Y., Nishimura, M., Adachi, T., Iwata, Y., and Yamazaki, Y., 1986, "Experimental Study of Rollover of LNG in Storage Tanks," Kawasaki Heavy Industries Technical Report (in Japanese), No.93, pp. 1-8.

Newell, T.A. and Von Driska, P.M., 1983, "Double Diffusive Convection across a Single Interface at High Density Stability Ratios," *Natural Convection in Enclosure - 1983*, HTD-Vol. 26, ASME, pp. 11-15.

Sarsten, J.A., 1972, "LNG Stratification and Rollover," *Pipeline and Gas Journal*, Vol. 199, pp. 37-39.

Shi, J. Q., 1990, "Numerical Modeling and Experimental Study of Rollover in Cryogenic Liquids and Liquid Freon", Ph.D. Thesis, University of Southampton, Southampton, England.

Sugawara, Y., Tashita, M., Yamagata, S., Tateiwa, M., Fujiwara, M., and Igarashi, K., 1984, "Experimental Study on LNG Rollover Using Liquid Freon," Mitsubishi Heavy Industries Technical Report (in Japanese), Vol. 21, No. 2, pp. 1-11.

Takao, S. and Narusawa, U., 1980, "An Experimental Study of Heat and Mass Transfer across a Diffusive Interface," *Int. J. Heat and Mass Transfer*, Vol. 23, pp. 1283-1285.

Turner, J.S., 1965, "The Coupled Turbulent Transports of Salt and Heat Across a Sharp Density Interface," *Int. J. Heat and Mass Transfer*, Vol. 8, pp. 759-767.

Turner, J.S., 1973, *Buoyancy Effects in Fluids*, Cambridge University Press, pp.251-287.

HTD-Vol. 317-1

Proceedings of the

ASME HEAT TRANSFER DIVISION

VOLUME 1

- BENCHMARK PROBLEMS OF HEAT TRANSFER ANALYSIS PROGRAMS
- HIGH HEAT FLUX THERMAL MANAGEMENT
- MODELING OF HEAT TRANSFER IN MULTI-PHASE SYSTEMS
- NATURAL AND MIXED CONVECTION
- NUMERICAL METHODS IN HEAT EXCHANGER DESIGN

presented at

THE 1995 ASME INTERNATIONAL
MECHANICAL ENGINEERING CONGRESS AND EXPOSITION
NOVEMBER 12–17, 1995
SAN FRANCISCO, CALIFORNIA

sponsored by

THE HEAT TRANSFER DIVISION, ASME

edited by

ROBERT J. COCHRAN
ENGINEERING SCIENCES CENTER

ROY E. HOGAN
ENGINEERING SCIENCES CENTER

ALI M. KHOUNSARY
ARGONNE NATIONAL LABORATORY

M. A. ESADIAN
FLORIDA INTERNATIONAL UNIVERSITY

M. KAVIANY
UNIVERSITY OF MICHIGAN

ROD W. DOUGLASS
EG&G

L. C. BURMEISTER
UNIVERSITY OF KANSAS

J. E. O'BRIEN
EG&G

R. L. MAHAJAN
UNIVERSITY OF COLORADO

T. S. CHEN
UNIVERSITY OF MISSOURI-ROLLA

W. J. BRYAN
ANSYS, INCORPORATED

T. CHOPIN
ANSYS, INCORPORATED

L. W. SAWNSON
HEAT TRANSFER RESEARCH, INCORPORATED

THE AMERICAN SOCIETY OF MECHANICAL ENGINEERS
UNITED ENGINEERING CENTER / 345 EAST 47TH STREET / NEW YORK, N.Y. 10017